Submitted to ADVANCED MATERIALS

DOI: 10.1002/((please add manuscript number))

Rapid and Nondestructive Identification of Polytypism and Stacking Sequences in Few-layer Molybdenum Diselenide by Raman Spectroscopy

Xin Lu, M. Iqbal Bakti Utama, Junhao Lin, Xin Luo, Yanyuan Zhao, Jun Zhang, Sokrates T. Pantelides, Wu Zhou, Su Ying Quek, and Qihua Xiong*

X. Lu, M. I. B. Utama, Dr. Y. Zhao, Dr. J. Zhang and Prof. Q. H. Xiong
Division of Physics and Applied Physics
School of Physical and Mathematical Sciences
Nanyang Technological University
Singapore 637371, Singapore
E-mail: qihua@ntu.edu.sg

Prof. Q. H. Xiong
NOVITAS, Nanoelectronics Centre of Excellence
School of Electrical and Electronic Engineering
Nanyang Technological University
Singapore 639798, Singapore

J. Lin and Prof. S. T. Pantelides
Department of Physics and Astronomy
Vanderbilt University, Nashville
TN 37235, USA

J. Lin, Prof. S. T. Pantelides and Dr. W. Zhou
Materials Science & Technology Division
Oak Ridge National Laboratory, Oak Ridge
TN 37831, USA

Dr. X. Luo and Prof. S. Y. Quek
Department of Physics
Centre for Advanced 2D Materials and Graphene Research Centre
National University of Singapore
Singapore 117546, Singapore

Dr. X. Luo
Institute of High Performance Computing
Singapore 138632, Singapore

Keywords: molybdenum diselenide, few-layer, stacking, polytypism, interlayer shear mode

Interest in transition metal dichalcogenides (TMDs, *e.g.*, MoS_2, WS_2, WSe_2, $MoTe_2$) has been heightened by novel physical phenomena emerging in their monolayer form, such as direct band gap (~1.8 eV in MoS_2),[1] strong photoluminescence (PL),[2] and valley polarization.[3] Field-effect transistors from monolayer MoS_2 have shown high on-off ratio as

well. However, monolayer TMDs devices are very sensitive to charged impurity scattering, resulting in low field-effect mobility in unencapsulated devices (mostly around 1-10 $cm^2V^{-1}s^{-1}$).[4] In contrast, few-layer TMDs exhibit higher mobility (> 100 $cm^2V^{-1}s^{-1}$) and larger density of states for high driving current.[5] Therefore, few-layer TMDs overcome the shortcomings of their monolayer form in some specific applications, such as gas sensors and integrated circuits.[6] Moreover, interlayer interactions in few-layer TMDs lead to layer-dependent electrical and optical properties. As a new degree of freedom, stacking in few-layer TMDs has been shown to affect the optical properties substantially, such as the degree of valley polarization in MoS_2[7] and the PL peak position in vertical heterostructures.[8] Current studies in few-layer TMDs mostly focus on the 2H stacking phase, which is the most stable structure at ambient condition. Hence, most structural studies on TMDs only address defects in the form of point defects and grain boundaries in monolayers,[9] without considering mixtures of phases and stacking combinations. An in-depth study of stacking phases in few-layer TMDs, including 1T, 2H, 3R, and/or their mixture is still lacking.

Here, we demonstrate the use of Raman scattering spectroscopy for rapid identification of stacking sequences and polytypism in few-layer $MoSe_2$ crystals. The $MoSe_2$ samples are produced either by scotch-tape exfoliation or vapor transport synthesis in a chemical vapor deposition (CVD) system. By observing the interlayer shear modes on low-frequency Raman spectroscopy, for the first time, we are able to correlate the Raman features with different stacking arrangements in few-layer $MoSe_2$. Scanning transmission electron microscopy (STEM) annular dark field (ADF) Z-contrast imaging further confirms the presence of various stacking arrangements in few-layer $MoSe_2$. We believe that the present work will stimulate future studies on the influence of stacking on the optical and electronic properties of atomically thin TMDs.

Figure 1a shows low magnification optical-microscopy images of as-grown few-layer $MoSe_2$ flakes. By combining optical contrast and atomic force microscopy (AFM) measurements,[10] we can determine that most of the as-grown few-layer $MoSe_2$ flakes have

thickness between 2-8 layers (L) and typical width of 5-30 μm. The zoom-in images of 2-4 L flakes are shown in **Figure 1b-1d**.

We first performed Raman studies on exfoliated $MoSe_2$ samples (2H stacking) under different polarization configurations, as shown in **Figure 2a-2d**. We observed that A_{1g} mode blue-shifts and E^1_{2g} red-shifts as the number of layers increases, in agreement with previous reports on TMDs.[2,11] The opposite shifting direction in these two modes is caused by surface effects, which refers to the larger Mo-Se force constants at the surface layer.[11b] Moreover, the absence of B^1_{2g} mode under cross $\bar{z}(xy)z$ polarization (Figure 2b) suggests that the B^1_{2g} mode originates from out-of-plane (breathing) vibration.[12] Our previous work has demonstrated that the Raman vibrational modes have polarization dependence: Shear (in-plane) modes are Raman active in both parallel $\bar{z}(xx)z$ and cross $\bar{z}(xy)z$ polarization configurations, but breathing modes are suppressed significantly in $\bar{z}(xy)z$ configuration.[13] However, Raman measurements on exfoliated 2H $MoSe_2$ show the same number of low-frequency peaks under both configurations (Figure 2c and 2d), indicating the "absence" of all interlayer breathing modes in exfoliated $MoSe_2$ samples. Meanwhile, the interlayer shear modes show similar trends to previous studies on MoS_2 and WSe_2.[13]

All of our exfoliated $MoSe_2$ samples are in 2H stacking as it is derived from a single crystal that is also of 2H stacking. Meanwhile, we have previously reported that 2H and 3R stacking can coexist in a bilayer film of CVD-grown $MoSe_2$.[14] However, sample limitation in terms of layer number and grain sizes have prohibited systematic studies of different stacking order *via* Raman spectroscopy. With the progress in $MoSe_2$ synthesis to produce flakes with high crystalline quality, larger grain sizes, and clear distinction of different layer number,[15] further studies on the implication of 2H and 3R stacking become possible.

In particular, we aim to correlate the stacking configuration and interlayer shear modes by conducting Raman measurements on CVD-grown $MoSe_2$ flakes under cross polarization. The high frequency region (220-360 cm^{-1}) is nearly identical to that from exfoliated 2H $MoSe_2$. The shifts of A_{1g} and E^1_{2g} at different layer number are also not pronounced since the

intralayer vibrational modes are less sensitive to thickness than the interlayer ones.[2,11,13] Thus, we only plotted the spectra taken from CVD-$MoSe_2$ with different number of layers in low frequency region (< 40 cm^{-1}, **Figure 2e**). Since different Raman features can be observed on the flakes with the same thickness due to different stacking, we only show the spectra with the maximum number of observable interlayer shear modes in each layer in Figure 2e. Compared with the interlayer shear modes from exfoliated 2H $MoSe_2$ (Figure 2d), the spectra from CVD-$MoSe_2$ samples unambiguously show additional peaks labeled as S_2 and S_4 (Figure 2e). Both of them are Raman-inactive in 2H stacking, however they show up in the CVD-$MoSe_2$ samples.

Before describing our further experimental results, let us discuss from the theoretical point of view. There are *N*-1 interlayer shear modes in *N* layer TMDs, but not all of them can be observed by Raman spectroscopy. For brevity, we hereafter refer to the interlayer shear modes as S_1, S_2, S_3, … starting from the highest frequency in the order of decreasing frequency. In 2H stacking, counting from the highest frequency, only the odd interlayer shear modes (S_1, S_3, S_5, …) are observable. The even modes (S_2, S_4 …) cannot be observed, but for different reasons in even layers and odd layers: S_2 and S_4 modes are Raman-inactive (*i.e.*, zero matrix elements of the Raman tensor) in even layers (2 L, 4 L, …); in contrast, although S_2 and S_4 modes are Raman active in odd few-layers (3 L, 5 L, …), they cannot be observed on the commonly-used back-scattering configuration due to polarization (the modes might be observable in other scattering configurations).[13] Moreover, the peak intensity of all the observable interlayer shear modes in 2H follows the trend of $I(S_1) > I(S_3) > I(S_5) > \ldots$ relative to each other, as shown in Figure 2d.

The relative peak intensity in 3R stacking follows the opposite trend to 2H stacking since observable modes at lower frequency have higher intensities, with the lowest frequency mode (S_{N-1}) having the highest intensity. As an example of even layer, the trend of intensity in 6 L is $I(S_1) > I(S_3) > I(S_5)$ in 2H stacking and $I(S_5) > I(S_3) > I(S_1)$ in 3R stacking. As an example of odd layer, the trend of intensity in 5 L follows $I(S_1) > I(S_3)$ in 2H stacking and $I(S_4) > I(S_2)$ in 3R stacking. Meanwhile, in 3R stacking, the alternate modes starting from the second lowest

frequency (S_{N-2}, for $N > 2$) are unobservable on back-scattering configuration (*e.g.*, S_4 and S_2 are unobservable in 6 L). The last commonly known phase, 1T, is considered as "metastable" in $MoSe_2$.[16] Thus, 1T-$MoSe_2$ is not expected to withstand high temperature CVD synthesis, and we will mainly focus on 2H and 3R, without discussing 1T stacking in this report.

The difference between 2H and 3R starts from bilayer in crystal structure. **Figure 3a** shows the schematic of 2H and 3R stackings in 2 L. In addition to the shift of the layer, which also happens in 3R stacking, the N^{th} layer of 2H stacking is rotated with respect to the N-1^{th} layer. Although the observable modes are different in 2H and 3R stackings, the energy of each phonon mode will not necessarily be different. From our density functional theory (DFT) calculations (**Figures 3b-3e**), the frequencies in 2H and 3R stacking have negligible difference in all S_1-S_4 modes (Normal mode displacements of S_1-S_4 modes in 2-5 L are shown in **Supporting Information Figure S1-S3**). The similar frequencies of S_1-S_4 modes in 2H and 3R stackings indicate that the force constant and the mass per unit area are insensitive to stacking. Moreover, we found that the experimental frequencies of the extra peaks in Figure 2e agree well with the calculated frequencies of the S_2 and S_4 modes, but DFT calculations cannot explain the origin of some modes, such as S_2 mode in 4 L. Neither 2H-stacked 4 L or 3R-stacked 4 L can give rise to S_2 mode. We therefore use a bond polarizability model to predict the Raman modes and intensity in $MoSe_2$ with stacking faults. In a separate work,[17] we have shown with bond polarizability analysis that the relative intensity of interlayer Raman modes can be determined from the space group and stacking order in the material. That analysis explains why some interlayer modes are never observed in certain materials although group theory predicts that the modes are Raman active. Applying the bond polarizability analysis here, we found that stacking faults can give new characteristics on the interlayer shear modes. For example, strong S_2 mode can occur in both ABCB and ABAC stacking in 4 L, *i.e.*, one or two layers deviated from the perfect positions in 3R stacking (ABCA). These predictions are also supported by the first principles calculations.

With such detailed theoretical support, we have conducted further measurements on flakes with different number of layers to substantiate our analysis**.** For 2 L $MoSe_2$, all CVD-

grown samples show a strong shear mode (S_1) around 19 cm^{-1}, with a full width at half maximum of 1.5 cm^{-1}, which is comparable to 1.0 cm^{-1} in exfoliated 2H bilayer (**Figure 4a**). Both 2H and 3R stackings have an active S_1 mode, which cannot be used to distinguish the stacking in bilayers. However, in 3 L and thicker layers, the emergence of interlayer shear modes becomes strongly stacking-dependent. According to our theoretical analysis as discussed previously, 3 L has only observable S_1 mode in 2H stacking and only observable S_2 mode in 3R stacking. Indeed, we observed flakes that exhibit such Raman features from CVD-$MoSe_2$ (**Figure 4b**), allowing us to assign the stacking of such flakes to be either 2H (~28%) or 3R (~35%, see **Figure 4f**). The coexistence of S_1 and S_2 modes is also observed on around 37% of all 3 L samples, which we attribute to the in-plane mixture of 2H and 3R phases in a single flake (*i.e.*, polytypism). This mixture can be either connected with a sharp boundary or through a gradual transition in lateral direction. Indeed, the mixture of 2H and 3R phases with atomically sharp boundary has been observed in our CVD-grown bilayer films (**Figure S4a**). To the best of our knowledge, this is the first report of polytypism in individual few-layer TMDs flakes. While the exact mechanism and origin of such polytypism are not fully understood in our samples, we speculate that polytypism is possible at high temperature synthesis since previous theoretical calculations show a very close formation energy between 2H and 3R stacking (0.3 meV/atom).[18]

Next, we address the Raman features observed in 4 L $MoSe_2$ (**Figure 4c**). As expected from calculations, the highest frequency peak (S_1) is dominant in 2H phase; in 3R stacking, the lowest frequency mode (*i.e.*, S_3 in 4 L) is the strongest. The emergence of the S_2 mode can be attributed to stacking fault, either ABCB or ABAC stacking. Among all the 4 L samples we have measured, 9.5% is assigned to be ABCB/ABAC stacking. However, 59.5% of 4 L CVD-$MoSe_2$ exhibited spectral features that cannot be simply assigned to only one form of stacking (blue lines in Figure 4c). Thus, we believe that these flakes have a mixture of phases. We categorize the 59.5% flakes into "2H-based (~30.5%)" and "3R-based (~29%)" mixture: the difference lies in the intensity of the S_3 mode. Since S_3 mode is the weakest in both 2H and ABCB/ABAC stackings, it is usually almost invisible in the measured spectra.[13]

However, S_3 mode is the strongest in 3R phase. The individual flakes with phase mixing of 3R stacking may still exhibit substantial intensity of S_3 mode.

More stacking combinations should be considered when we add one more layer to reach 5 L (**Figure 4d**). Similar to 3 L, 2H (S_1-dominant) and 3R (S_4-dominant) can be assigned unambiguously. However, many different combinations of Raman features remain. For instance, S_3-dominant samples constitute 17% of all 5 L CVD-$MoSe_2$. According to our calculations, ABCBA stacking has enhanced S_3 mode, with negligible S_1, and Raman-inactive S_2 and S_4 modes. Similarly, we have assigned ABACA (S_2-dominant) and ABABC/ABCBC stacking with $I(S_1) > I(S_2) > I(S_3) > I(S_4)$ in Figure 3h.

To further confirm our analysis on the correlations between the interlayer shear modes and stacking, we performed ADF Z-contrast imaging in an aberration-corrected STEM to study the atomic structure of the few-layer CVD-$MoSe_2$. **Figure 5a** shows a Z-contrast image of bilayer $MoSe_2$ in 3R stacking. The intensity at each atomic site in Z-contrast images is correlated to the atomic number and the number of atoms in the imaged atomic columns.[19] 3R stacking in bilayer $MoSe_2$ can be unambiguously determined by the image intensity, where the overlapping sites (Mo+Se_2, bright spots) are surrounded by Mo and Se_2 column from the top and bottom layers (dim spots), as shown in the intensity profile. In contrast, 2H stacking in bilayer maintains the hexagonal shape and has equal intensity in each atomic site.[18] Z-contrast images of 3 L and 4 L $MoSe_2$ in 3R stacking are shown in **Figure 5b** and **5c**, respectively, in agreement with the simulated images using the perfect 3R stacking model. We found that 3R stacking is more frequently observed than 2H stacking in the multilayer flakes, consistent with the statistical analysis in Figure 4e-4h. Meanwhile, it is also an indication that 3R is slightly more preferable than 2H during our synthesis, although 2H phase is more commonly seen in nature.

In addition to the perfect 2H and 3R stackings, we also observed flakes with "shifted" 2H (**Figure 5d**: 8 L) and 3R (**Figure 5e**: a flake with 1–5 L region) stacking. The term "shifted" means that one or more layers in the few-layer flakes have a slight interlayer shift from the perfect 2H or 3R stacking positions without any misorientation, as confirmed by the fast

Fourier transform (FFT) of the ADF image. For example, by comparing with the simulated image of a "shifted" 3R stacking model structure (Figure 5e inset) near the edge region, we found that the shifting occurred in the <100> direction with different amount of shifting distance in each layer. We estimated the amount of shift as 0.4 Å in 2nd L, 0.8 Å in 3rd L, 1.2 Å in 4th L, and 1.6 Å in 5th L. Although the 5th layer is ~57% away from the perfect 3R stacking positions ($MoSe_2$ lattice spacing $d_{\{100\}}$: 2.8 Å, where the lattice constant a: 3.3 Å[20]). Our theoretical calculations show that the relatively small interlayer shifting (*i.e.*, 0.4 Å between adjacent layer, ~14% of $d_{\{100\}}$) should not create significant changes in the interlayer shear modes on the Raman spectra. These results suggest that the previously observed Raman spectrum labelled with 2H and 3R stacking may also involve the contribution from "shifted" 2H and 3R stacking. Direct evidence showing the co-existence of "shifted" 2H and 3R stacking (*i.e.*, polytypism) is provided in **Figure S4b-S4e**.

However, as the interlayer shifting increases, the layer may register into different atomic sites and generate local stacking faults inside the flake, resulting in new Raman features. For example, ABCB stacking leads to the emergence of S_2 mode in Raman spectra in 4 L $MoSe_2$. In order to achieve ABCB (stacking fault) from ABCA (perfect 3R stacking) locally, one has to shift all the atoms in the 4th layer from A sites to B sites, resulting in a interlayer shifting of ~50%. Indeed, transition regions between different stackings were observed in our CVD-$MoSe_2$ sample. **Figure 5f** shows a Z-contrast image of one side of the transition region in a 5 L flake with the well-aligned 3R stacking on the right. The image shows that one or more layers are gradually shifting (either stretching or compressing) without rotation and mis-orientation, as confirmed by the FFT (inset). The transition regions have a typical width of hundreds of nanometers. Such gradual transition of stacking which generates local stacking faults may be due to out-of-plane fluctuations between layers.[21] This observation confirms our analysis of the new Raman features which can be correlated to a mixture of phases and polytypism.

It should be noted that due to the projective nature of STEM imaging, it is difficult to unambiguously identify the exact stacking sequence from the images. For example, 4 L

$MoSe_2$ with ABAC and ABCA stacking could generate very similar STEM ADF images (**Figure S5a** and **S5b)**. However, ABAC and ABCA could be easily distinguished from their distinct Raman features: S_2 mode dominates ABAC while S_3 mode is the strongest in ABCA. This further establishes that Raman spectroscopy is indeed an important tool in studying the stacking of TMDs.

In addition to polytypism in the in-plane direction, we also remark that out-of-plane mixture of phases may also result in the emergence of additional shear mode combinations. For example, we conducted DFT calculation in a fully relaxed 3 L $MoSe_2$ with the first two layers in 2H phase and the topmost layer in 3R phase. Our calculation shows that both S_1 and S_2 shear modes would be IR and Raman active, similar to cases of in-plane mixture (Fig. 4b, blue curve). However, our STEM observations have not found such out-of-plane mixture in our CVD-grown samples and as such, we have excluded the variant of phase mixture in our discussions.

To conclude, few-layer $MoSe_2$ flakes are synthesized by CVD. New features, especially modes that are Raman-inactive in 2H phase, emerge in the CVD-grown samples. We have identified the new modes by confirming the peak positions *via* first-principles calculations. A bond polarizability model, described elsewhere for general layered materials,[17] was then used to explore the influence of stacking sequence on Raman features. We demonstrate the relation between stacking and interlayer shear modes on Raman spectroscopy. STEM-ADF Z-contrast imaging confirms the presence of various stacking arrangements in few-layer $MoSe_2$. For the first time, stacking faults and polytypism are reported in CVD-grown flakes of few-layer TMDs and correlated with Raman spectroscopy. As we have proposed herein, Raman spectroscopy is a reliable tool to investigate the stacking configuration of TMDs rapidly and non-destructively. We believe that the correlation of stacking sequence and polytypism to the low-frequency Raman properties should also be applicable to other members of the TMDs family because of the similarity in crystal structure and optical properties. We hope that this work will motivate further systematic studies of stacking-dependent properties, which are important for future applications based on few-layer TMDs and 2D heterostructures.

Experimental Section

We adopt the selenization method in our CVD growth of $MoSe_2$.[14] Few-layer $MoSe_2$ flakes were synthesized in a single-zone vapor transport CVD system with a quartz tube reactor. Si substrate capped with 285 nm thermal SiO_2 was put upside down on the center boat, which contains MoO_3 powder. The boat with Se powder is placed 15.5 cm away from the center. The temperature was elevated to 750°C in 15 minutes, maintained for 5 minutes, and reduced naturally to room temperature. During growth, the whole system was kept at 810 Torr with 20 sccm of 5% H_2/Ar as the carrier gas. Details on the growth setup and electrical properties of CVD-$MoSe_2$ flakes were discussed in our previous paper.[15]

The as-grown CVD-$MoSe_2$ flakes were characterized using optical microscope (Olympus BX51) and AFM (Veeco Dimension V) in a tapping mode. Afterwards, Raman measurements were conducted on a triple-grating micro-Raman spectrometer (Horiba-JY T64000) under back scattering configuration. Excitation laser was 532 nm and the laser power was kept low to avoid possible damage and oxidation on the samples. The signal was collected through a 100× objective, dispersed with a 1800 g/mm grating, and detected by a charge-coupled device cooled by liquid nitrogen. ADF Z-contrast imaging was performed on a Nion UltraSTEM 100 operated at 100 kV. The convergence semi-angle is set to be ~ 30 mrad. ADF images were acquired from the ~ 80-200 mrad range. The sample was baked in a vacuum chamber at 160˚C before being inserted into the microscope in order to reduce contaminations.

First-principles calculations of vibrational Raman spectra are performed within density functional theory (DFT) as implemented in the plane-wave pseudopotential code QUANTUM-ESPRESSO. The local density approximation (LDA) to the exchange-correlation functional is employed in the norm-conserving pseudopotential throughout the Raman spectra calculation. To get converged results, plane-wave kinetic energy cutoffs of 65 Ry are used for the wave functions. The slabs are separated by 16 Å of vacuum to prevent interactions between slabs (this value has been tested for convergence of phonon frequencies). A Monkhorst-Pack *k*-point mesh of 17×17×1 is used to sample the Brillouin Zones for the thin films. The structures are considered as relaxed when the maximum component of the Hellmann-Feynman force acting on each ion is less than 0.003 eV/Å. With the optimized structures and self-consistent wave functions, the phonon spectra and Raman intensities are calculated within density-functional perturbation theory (DFPT) as introduced by Lazzeri and Mauri.[22] Details of the bond polarizability analysis are given in [17].

Supporting Information

Supporting Information is available from the Wiley Online Library or from the author.

Acknowledgements
Q.X. gratefully thanks Singapore National Research Foundation *via* a Fellowship grant (NRF-RF2009-06) and an Investigatorship grant (NRF-NRFI2015-03), Ministry of Education *via* a tier2 grant (MOE2012-T2-2-086) and a tier1 grant (2013-T1-002-232). S.Y.Q. and X.L. gratefully acknowledges the Singapore National Research Foundation (NRF) for funding under the NRF Fellowship (NRF-NRFF2013-07). The computations were performed on the cluster of NUS Graphene Research Centre. This research was supported in part by U.S. DOE grant DE-FG02-09ER46554 (J.L., S.T.P.), by the Office of Science, Basic Energy Science, Materials Sciences and Engineering Division, U.S. Department of Energy (W.Z.), and through a user project supported by ORNL's Center for Nanophase Materials Sciences (CNMS), which is sponsored by the Scientific User Facilities Division, Office of Basic Energy Sciences, U.S. DOE.

Received: ((will be filled in by the editorial staff))
Revised: ((will be filled in by the editorial staff))
Published online: ((will be filled in by the editorial staff))

[1] K. F. Mak, C. Lee, J. Hone, J. Shan, T. F. Heinz, *Phys. Rev. Lett*. **2010**, *105*, 136805.

[2] P. Tonndorf, R. Schmidt, P. Boettger, X. Zhang, J. Boerner, A. Liebig, M. Albrecht, C. Kloc, O. Gordan, D. R. T. Zahn, S. M. de Vasconcellos, R. Bratschitsch, *Opt. Express* **2013**, *21*, 4908.

[3] a) H. Zeng, J. Dai, W. Yao, D. Xiao, X. Cui, *Nat. Nanotechnol.* **2012**, *7*, 490; b) K. F. Mak, K. He, J. Shan, T. F. Heinz, *Nat. Nanotechnol.* **2012**, *7*, 494; c) T. Cao, G. Wang, W. Han, H. Ye, C. Zhu, J. Shi, Q. Niu, P. Tan, E. Wang, B. Liu, J. Feng, *Nat. Commun.* **2012**, *3*, 887.

[4] Q. H. Wang, K. Kalantar-Zadeh, A. Kis, J. N. Coleman, M. S. Strano, *Nat. Nanotechnol.* **2012**, *7*, 699.

[5] S. Kim, A. Konar, W. S. Hwang, J. H. Lee, J. Lee, J. Yang, C. Jung, H. Kim, J. B. Yoo, J. Y. Choi, Y. W. Jin, S. Y. Lee, D. Jena, W. Choi, K. Kim, *Nat. Commun.* **2012**, *3*, 1011.

[6] a) H. Li, Z. Yin, Q. He, X. Huang, G. Lu, D. W. Fam, A. I. Tok, Q. Zhang, H. Zhang, *Small* **2012**, *8*, 63; b) H. Wang, L. Yu, Y. H. Lee, Y. Shi, A. Hsu, M. L. Chin, L. J. Li, M. Dubey, J. Kong, T. Palacios, *Nano Lett.* **2012**, *12*, 4674.

[7] T. Jiang, H. Liu, D. Huang, S. Zhang, Y. Li, X. Gong, Y. R. Shen, W. T. Liu, S. Wu, *Nat. Nanotechnol.* **2014**, *9*, 825.

[8] H. Fang, C. Battaglia, C. Carraro, S. Nemsak, B. Ozdol, J. S. Kang, H. A. Bechtel, S. B. Desai, F. Kronast, A. A. Unal, G. Conti, C. Conlon, G. K. Palsson, M. C. Martin, A. M. Minor, C. S. Fadley, E. Yablonovitch, R. Maboudian, A. Javey, *Proc. Nat. Acad. Sci.* **2014,**

111, 6198.

[9] W. Zhou, X. Zou, S. Najmaei, Z. Liu, Y. Shi, J. Kong, J. Lou, P. M. Ajayan, B. I. Yakobson, J. C. Idrobo, *Nano Lett*. **2013**, *13*, 2615.

[10] a) H. Li, J. Wu, X. Huang, G. Lu, J. Yang, X. Lu, Q. Zhang, H. Zhang, *ACS Nano* **2013**, *7*, 10344; b) X. Lu, M. I. B. Utama, J. Zhang, Y. Zhao, Q. H. Xiong, *Nanoscale* **2013,** *5*, 8904.

[11] a) C. Lee, H. Yan, L. E. Brus, T. F. Heinz, J. Hone, S. Ryu, *ACS Nano* **2010**, *4*, 2695; b) X. Luo, Y. Zhao, J. Zhang, Q. Xiong, S. Y. Quek, *Phys. Rev. B* **2013**, *88*, 075320.

[12] X. Luo, Y. Zhao, J. Zhang, M. Toh, C. Kloc, Q. H. Xiong, S. Y. Quek, *Phys. Rev. B* **2013**, *88*, 195313.

[13] Y. Zhao, X. Luo, H. Li, J. Zhang, P. T. Araujo, C. K. Gan, J. Wu, H. Zhang, S. Y. Quek, M. S. Dresselhaus, Q.H. Xiong, *Nano Lett*. **2013**, *13*, 1007.

[14] a) X. Lu, M. I. B. Utama, J. Lin, X. Gong, J. Zhang, Y. Zhao, S. T. Pantelides, J. Wang, Z. Dong, Z. Liu, W. Zhou, Q. H. Xiong, *Nano Lett.* **2014**, *14*, 2419; M. I. B. Utama, X. Lu, D. Zhan, S. T. Ha, Y. Yuan, Z. Shen, Q. H. Xiong, *Nanoscale* **2014**, *6*, 12376.

[15] M. I. B. Utama, X. Lu, Y. Yuan, Q. H. Xiong, *Appl. Phys. Lett.* **2014**, *105*, 253102.

[16] U. Gupta, B. S. Naidu, U. Maitra, A. Singh, S. N. Shirodkar, U. V. Waghmare, C. N. R. Rao, *APL Mater*. **2014**, 2, 092802.

[17] X. Luo, C. Cong, X. Lu, T. Yu, Q. H. Xiong, S. Y. Quek, Stacking sequence determines Raman intensities of observed interlayer shear modes in 2D layered materials – A general bond polarizability model, arXiv:1504.04927.

[18] a) J. He, K. Hummer, C. Franchini, *Phys. Rev. B* **2014**, *89*, 075409; b) Q. Liu, L. Li, Y. Li, Z. Gao, Z. Chen, J. Lu, *J. Phys. Chem. C* **2012,** *116*, 21556.

[19] P. D. Nellist, In *Scanning transmission electron microscopy: Imaging and analysis* Eds: S. J. Pennycook, P. D. Nellist, Springer, New York, USA, 2011, 91−115.

[20] R. Coehoorn, C. Haas, J. Dijkstra, C. J. F. Flipse, R. A. Degroot, A. Wold, *Phys. Rev. B* **1987**, *35*, 6195.

[21] J. Lin, W. Fang, W. Zhou, A. R. Lupini, J. C. Idrobo, J. Kong, S. J. Pennycook, S. T. Pantelides, *Nano Lett.* **2013**, *13*, 3262.

[22] M. Lazzeri, F. Mauri, *Phys. Rev. Lett.* **2003**, *90*, 036401.

Figure 1

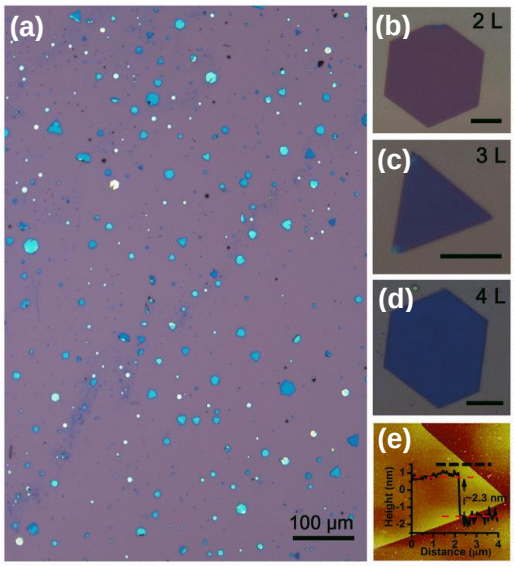

Figure 1. CVD-grown few-layer $MoSe_2$ flakes on Si substrate capped with 285 nm SiO_2. (a) Low magnification optical image of the as-grown $MoSe_2$ flakes. (b)-(d) Optical images of individual few-layer $MoSe_2$ flakes. Layer numbers are shown on the top right corner. Scale bars correspond to 10 μm. (e) AFM image of the $MoSe_2$ flake in (b). Height profile indicates that the layer number is three.

Figure 2

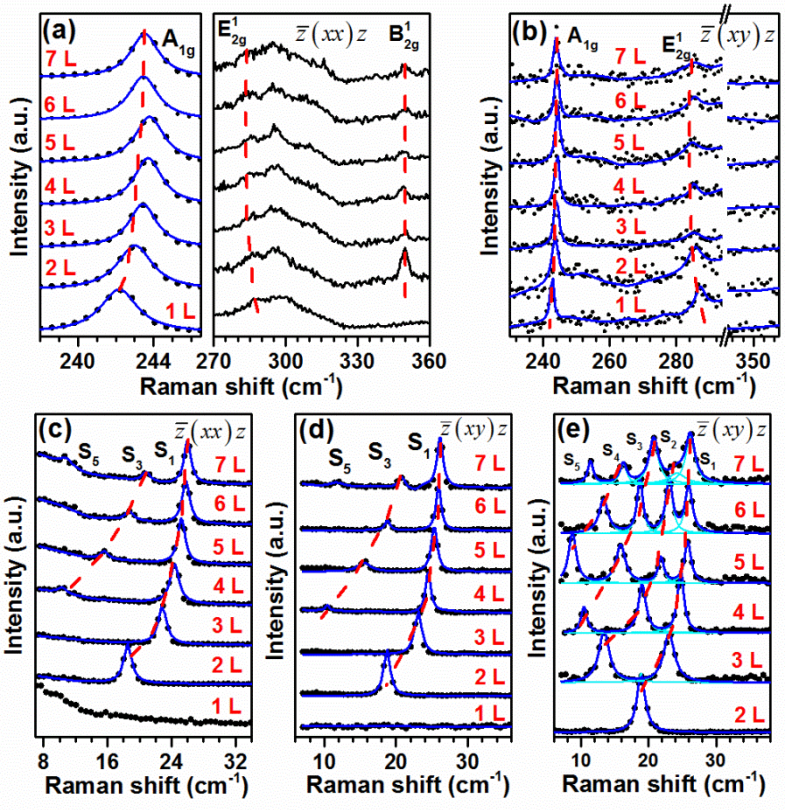

Figure 2. (a-d) Raman spectra of exfoliated monolayer and few-layer $MoSe_2$, in high-frequency (220-360 cm^{-1}) and low frequency region (< 40 cm^{-1}) under both parallel $\bar{z}(xx)z$ and cross $\bar{z}(xy)z$ polarization. In (a-d), black lines/dots are experimental data, and blue lines are fitting results using Lorentzian function. (e) Low-frequency Raman spectra of few-layer CVD-$MoSe_2$ under $\bar{z}(xy)z$ configuration.

Figure 3

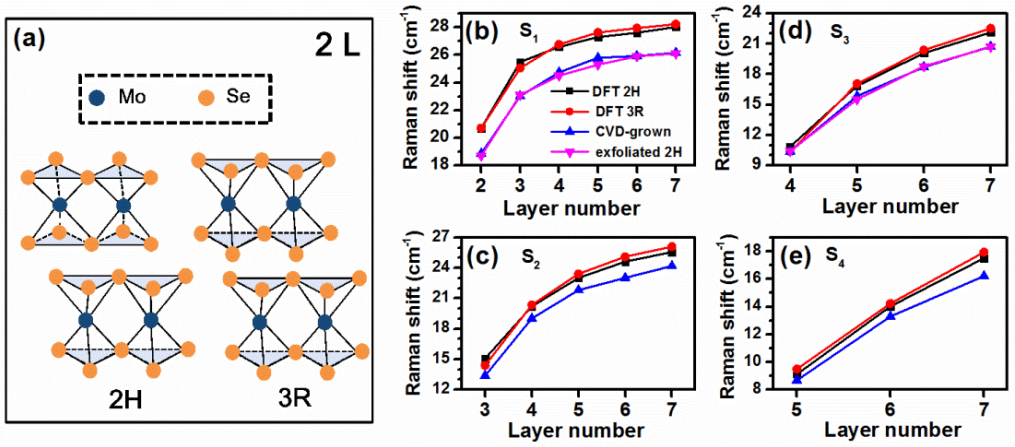

Figure 3. (a) Schematic of 2H and 3R stackings in 2 L. (b)-(e) Thickness-dependent frequencies of interlayer shear modes obtained from first principles calculations and experiments. "DFT 2H" (3R) means refers to the frequencies are from DFT calculations on 2H (3R) stacking, as displayed in black (red) in the figures. Experimental data from CVD-grown (blue) and exfoliated 2H (magenta) samples flakes are also included.

Figure 4

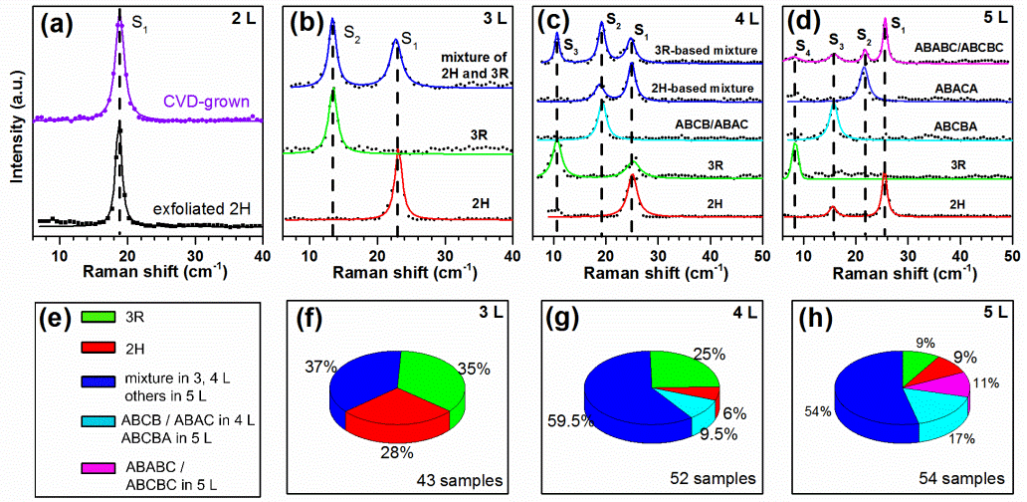

Figure 4. (a) Low-frequency Raman spectra of CVD-grown and 2H-exfoliated $MoSe_2$ bilayers. (b-d) Low-frequency Raman spectra of CVD-grown 3 L (b), 4 L (c), and 5 L (d) $MoSe_2$ samples with different stacking. Dots in (a-d) are experimental data and solid lines are fitting results using Lorentzian function. (e-h) Pie charts of 3 L (f), 4 L (g), and 5 L (h), which show the proportion of different stackings in a given thickness. The legend is shown in (e).

Figure 5

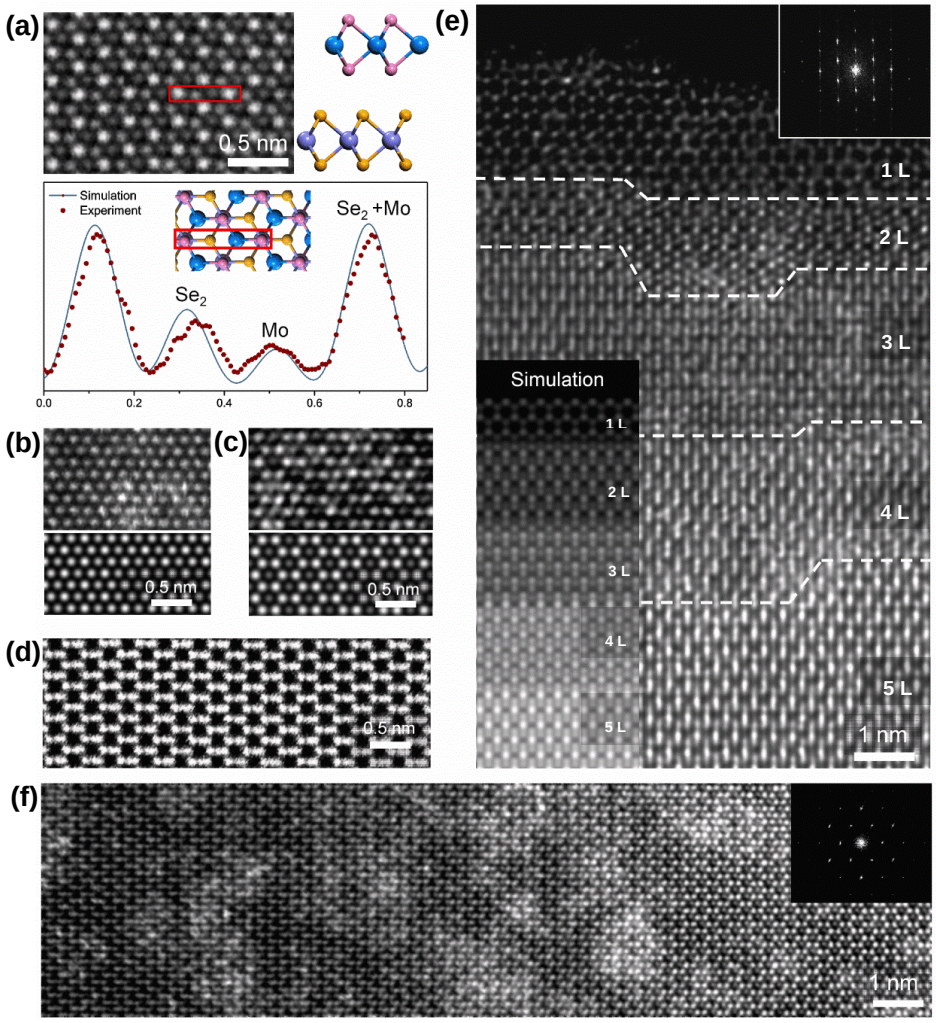

Figure 5. Z-contrast imaging of stacking in the as-grown few-layer $MoSe_2$. (a) Atomic resolution image and side-view scheme of 3R stacking in bilayer $MoSe_2$. The plot shows the intensity profile of the highlighted atomic columns in (a). Inset of the plot: Schematic of the imaged region. (b,c) 3R stacking in 3 L (b) and 4 L (c), respectively. The simulated images are provided in the lower row. (d) Shifted-2H stacking in an 8 L sample. (e) Shifted-3R stacking in a flake with 1-5 L region. Top inset: FFT of the image. Lower inset: Simulated image of the shifted-3R stacking with 0.4 Å interlayer shift from the perfect 3R stacking. (f) Continuous shifting of one (or more) layer away from the perfect-3R stacking (right side) in a 5 L flake. Such shift might create mixtures of different stacking sequence within the same flake. Inset: FFT of the image.

The table of contents (50−60 words)

Various combinations of interlayer shear modes emerge in few-layer molybdenum diselenide ($MoSe_2$) grown by chemical vapor deposition depending on the stacking configuration of the sample. Raman measurements may also reveal polytypism and stacking fault, as supported by first principles calculations and high-resolution transmission electron microscopy. Thus, Raman spectroscopy is an important tool in probing stacking-dependent properties in few-layer 2D materials.

Keywords: molybdenum diselenide, few-layer, stacking, polytypism, interlayer shear mode

Xin Lu, M. Iqbal Bakti Utama, Junhao Lin, Xin Luo, Yanyuan Zhao, Jun Zhang, Sokrates T. Pantelides, Wu Zhou, Su Ying Quek, and Qihua Xiong*

Title: Rapid and Nondestructive Identification of Polytypism and Stacking Sequences in Few-layer Molybdenum Diselenide by Raman Spectroscopy

ToC figure (55 mm broad × 50 mm high)